IEEE Access
Multidisciplinary ⋮ Rapid Review ⋮ Open Access Journal

Received May 18, 2020, accepted May 28, 2020, date of publication June 8, 2020, date of current version June 22, 2020.

Digital Object Identifier 10.1109/ACCESS.2020.3000796

Robust Detection of Presence of Individuals in an Indoor Environment Using IR-UWB Radar

JI-EUN KIM, JAE-HO CHOI, AND KYUNG-TAE KIM
Department of Electrical Engineering, Pohang University of Science and Technology, Pohang 37673, South Korea

Corresponding author: Kyung-Tae Kim (kkt@postech.ac.kr)

This research was supported by Energy Cloud R&D Program through the National Research Foundation of Korea (NRF) funded by the Ministry of Science, ICT (NRF-2019M3F2A1073402).

ABSTRACT In this paper, we propose a robust detection method to determine the presence of individuals in an indoor environment by exploiting an impulse-radio ultra-wideband (IR-UWB) radar. Detection of the presence of individuals in an indoor environment using IR-UWB is not a trivial problem because real indoor environments provide heavy clutter components and spurious ones due to multipath effects. The study mainly discusses two difficulties involved in detecting an individual in an indoor environment, namely, how to reduce the clutter in an indoor environment and how to detect a very low radar cross section (RCS) target, i.e., an individual lying down. To reduce clutter components in indoor environments, we investigated several clutter reduction techniques in terms of detecting a standing individual and an individual lying down. However, even after clutter reduction, detection of an individual lying down continues to pose a challenge. Thus, we devised a novel two-stage detection scheme that first involves detection in the range domain, and then in the frequency domain, thereby resulting in good detection performance in terms of a high detection rate and a low false alarm rate. The proposed method was demonstrated by experiments in indoor environments, and the results indicate that its performance is robust in various scenarios.

INDEX TERMS Human detection, IoT sensor, smart-home, ultra-wideband (UWB) radar, vital signs.

I. INTRODUCTION

Impulse-radio ultra-wideband (IR-UWB) radar is widely used to detect or track humans due to its ability to penetrate obstacles and to resolve small range variation [1]. The sensor is characterized by sequentially transmitting several very short pulses [2] and provides extremely high-resolution in range direction. This attribute makes it possible to resolve the displacement of a few centimeters, even generated by very small movements of humans [3]. Hence, it enables us to determine the precise position of humans [4], and thus several studies focused on the use of IR-UWB for tracking [5]–[8], counting [9], [10], human gesture recognition [11], [12], and monitoring of individuals in an indoor or outdoor environment [13]–[15]. Thus, IR-UWB sensors have a variety of applications in areas such as security, internet-of-things (IoT) sensors, smart-home systems, health care systems, smart energy technologies, and automotive industry [16], [17].

IR-UWB radar can obtain information on humans, which is exploited for several purposes. For example, the position of human, direction of movement, and the number of individuals can promote the development of several future services such as controlling energy systems, home appliances, and security systems. These services will be utilized in exhibition halls, office buildings, commercial complexes, and individual housing [18]. Specifically, the information on the density and direction of individuals aids in organizing the placement of advertisements and tour schedules. In addition, human behavior analysis can be conducted with big data consisting of various radar signatures [19], [20]. Meanwhile, IR-UWB radar can detect vital signs of humans such as heartbeat and respiration rate [21]–[27]. Vital signs are generally used for noncontact monitoring of human in smart-home and hospitals [28]. After analyzing the collected vital signs data, the user can obtain the report of his/her health condition and proper prescription. In the automotive industry, IR-UWB radar is usually exploited for detection of pedestrians or other vehicles in advanced driver assistance systems (ADAS) [29], [30].

This paper focuses only on the detection of presence of individuals in an indoor environment. Hence, we devise a robust technique to detect the presence of individuals that

The associate editor coordinating the review of this manuscript and approving it for publication was Chengpeng Hao.

consists of two sequential steps, namely detection of a standing individual and that of an individual lying down. Several studies examined the use of IR-UWB radar for detection of vital signs including respiration rate and heart rate [21]–[27] and tracking and counting of individuals [5]–[10]. Vital signs detection is aimed at observing a single individual with limited motions. Most of the related experiments were performed in a very proximate distance between radar and human. Hence, the detection of presence of individuals is not sufficiently verified.

Individual tracking and counting usually require a complicated Kalman filtering and machine learning approach, respectively. Even though tracking and counting include the detection problem in an implicit manner, it is computationally inefficient in terms of detection of presence of an individual. Recently, there is an increasing demand for applications using information only about presence of individuals with low computational complexity. However, many studies on human detection have not been sufficiently or systematically investigated. Moreover, they have not been dealing with the problem of detection for individuals lying down in detail. To the best of our knowledge, our study first provides a systematic and detailed analysis of clutter reduction techniques concerning only human detection, and based on this investigation, we suggest a reasonable solution to this issue via the efficient combination of well-known techniques.

Nowadays, various fields of industry and society have focused on a reliable technique to detect the presence of individuals in an indoor environment because the accurate judgment of presence of individuals can save children trapped in a vehicle/building. Additionally, heating and lighting system in smart-home necessitates a simple and cheap sensor system that immediately responds to the presence of an individual to improve the energy efficiency. The proposed detection technique in this paper in conjunction with a radar sensor can be a good solution to the aforementioned applications in terms of cost and efficiency. Among various kinds of radar sensors, IR-UWB radar with a single-input single-output system is chosen due to its low cost and complexity. Furthermore, when compared to vision sensors, it does not involve a privacy problem, and it operates irrespective of weather or lighting conditions whether it is bright or dark [31], [32].

The proposed method is composed of two processing steps, which are sequentially connected to each other. The first step is to detect a standing individual in an indoor environment. The individual to be detected is assumed as standing, and thus a well-known constant false alarm (CFAR) technique in the range domain can provide good detection results due to relatively large radar cross section (RCS) of a standing individual. However, conventional CFAR techniques typically fail to detect an individual lying down because RCS of the individual is very low. Therefore, even when a standing individual is not detected in the first step, it is necessary to further determine whether or not a lying down individual exists. Hence, in the second step, the existence of an individual lying down is determined by using the CFAR technique in the frequency domain in order to detect the respiratory movement of a human. In advance of detection, to improve and guarantee good detection performance in an indoor environment, we should adopt appropriate processing techniques to mitigate clutter and multipath echoes as suitable for the first-and second-step, respectively. The performance of the proposed method was evaluated by conducting experiments with realistic scenarios in a room.

This paper is organized as follows. Section II describes the main proposed method. First, clutter reduction methods are compared in terms of detection of a standing individual. Subsequently, the detection of a standing individual is presented. Thereafter, two-stage detection for detection of an individual lying down is depicted. Finally, we present the overall detection scheme, which is a sequential combination of detection of a standing individual and that of an individual lying down with optimal clutter reduction methods. Section III shows the experiments with actual scenarios conducted under two types of indoor environments, namely normal clutter and heavy clutter. Finally, we conclude the paper in Section IV.

II. PROPOSED METHOD

A. RECEIVED SIGNAL

The received signal consists of three different components as follows:

$$x(t) = x_T(t) + x_C(t) + x_N(t), \tag{1}$$

where $x_T(t)$ denotes directly returned and multipath echoes due to a target, i.e., an individual, which includes single and direct reflections from the individual and also multiple reflections between the individual and stationary clutter. Specifically, $x_C(t)$ denotes the returned echo due to multiple reflections among stationary clutter and single and direct reflections from the clutter, and $x_N(t)$ denotes the measurement noise [22], [24]. Especially, indoor environments with ceiling, floor, and walls can lead to strong multiple reflections of RF signal, and the received signal $x(t)$ is significantly affected by the multipath effect. Thus, we noted that $x_T(t)$ and $x_C(t)$ include both types of reflection mechanisms, i.e., direct and multiple reflections.

After sampling in the range domain for the i^{th} transmitting pulse, the received signal is expressed as follows:

$$\mathbf{x}_i = \left[x_{i1} x_{i2} \ldots x_{ij} \ldots x_{i,n_r}\right]^T, \tag{2}$$

where n_r denotes the number of sampling range bin, and x_{ij} denotes the component of the j^{th} sampling range bin of the i^{th} received pulse. If we collect $\boldsymbol{n}_p$ pulses, which are referred to as a single frame, then the $\boldsymbol{n}_r \times \boldsymbol{n}_p$ matrix $\mathbf{X}$ can be described as follows:

$$\mathbf{X} = \left[\mathbf{x}_1 \mathbf{x}_2 \ldots \mathbf{x}_i \ldots \mathbf{x}_{n_p}\right] = \begin{pmatrix} \boldsymbol{x}_{11} & \cdots & \boldsymbol{x}_{n_p,1} \\ \vdots & \ddots & \vdots \\ \boldsymbol{x}_{1,n_r} & \cdots & \boldsymbol{x}_{n_p,n_r} \end{pmatrix}.$$
$$\boldsymbol{i} = 1, 2, \ldots, \boldsymbol{n}_p$$
$$\boldsymbol{j} = 1, 2, \ldots, \boldsymbol{n}_r \tag{3}$$

B. DETECTION OF A STANDING INDIVIDUAL

1) NORMALIZATION

In order to detect the presence of an individual in a heavy clutter environment, the received signals should be normalized to compensate system instability. Generally, the received signals using the IR-UWB radar fluctuate from pulse to pulse due to instability of radio frequency (RF) hardware such as oscillators, low noise amplifiers (LNAs), and transmission lines. In particular, the fluctuations significantly degrade the performance of a clutter reduction part, which is an essential process to detect an individual in an indoor environment. Thus, we adopt a signal normalization process to handle the pulse-to-pulse fluctuations as follows [33]:

$$\begin{aligned} \bar{x}_{ij} &= \frac{x_{ij} - x_{i,min}}{x_{i,max} - x_{i,min}}, \\ i &= 1, 2, \ldots, n_p \\ j &= 1, 2, \ldots, n_r \end{aligned} \tag{4}$$

where

$$\begin{aligned} x_{i,min} &= \min x_{ij}, \quad \mathbf{j} = 1, 2, \ldots, n_r \text{ for a given } i \\ x_{i,max} &= \max x_{ij}, \quad \mathbf{j} = 1, 2, \ldots, n_r \text{ for a given } i. \end{aligned}$$

The normalization process in (4) can ensure that the sample values in every received pulse are between zero and one. Hence, the i^{th} normalized received signal $\bar{\mathbf{x}}_i$ and normalized matrix $\overline{\mathbf{X}}$ in a single frame consisting of n_p pulses are established as follows:

$$\begin{aligned} \bar{\mathbf{x}}_i &= \left[\bar{x}_{i1}\bar{x}_{i2} \ldots \bar{x}_{ij} \ldots \bar{x}_{i,n_r}\right]^T, \\ \overline{\mathbf{X}} &= \left[\bar{\mathbf{x}}_1\bar{\mathbf{x}}_2 \ldots \bar{\mathbf{x}}_i \ldots \bar{\mathbf{x}}_{n_p}\right] = \begin{bmatrix} \bar{x}_{11} & \cdots & \bar{x}_{n_p,1} \\ \vdots & \ddots & \vdots \\ \bar{x}_{1,n_r} & \cdots & \bar{x}_{n_p,n_r} \end{bmatrix}. \\ i &= 1, 2, \ldots, n_p \\ j &= 1, 2, \ldots, n_r \end{aligned} \tag{5}$$

The normalized matrix $\overline{\mathbf{X}}$ consisting of n_p normalized received pulses will be an input to the proposed method

2) CLUTTER REDUCTION

In an indoor environment, returned echoes of the desired target, i.e., an individual, are much weaker than those of clutter that originate from furniture and home appliances with larger RCS than humans in most cases. Fig. 1a illustrates the measured echoes from an individual; these echoes were obtained in a room, as shown in Fig. 1b. This room (4.5 m × 9.5 m) contained a TV, several tables, and chairs; hence, there were significant clutter components in the received echoes. The black line is referred to as "empty room echo" in our paper corresponds to results with only clutter and without any individual, while the blue and red lines correspond to those with a stationary (i.e., standing and stationary) individual at a range of 3 m and with a moving (i.e., standing and moving) individual within 3 m, respectively.

As shown in Fig. 1a, a very high peak at around 0 m is observed because a direct leakage signal exists from the transmitting antenna to the receiving antenna. In addition, at ranges higher than 1 m, small fluctuations exist due to clutter and multipath effect for the black line in Fig. 1a, while the red and blue lines show very small echoes from an individual in addition to those from clutter and multipath. A comparison of the signal corresponding to a stationary individual (the blue line) and an empty room echo (the black line) in Fig. 1a indicates that the blue line has several high peaks due to an individual at around 3 m. However, the peaks are smaller than the surrounding clutter. Furthermore, in the case of the moving individual (the red line in Fig. 1a), it is almost impossible to distinguish the returned echo from the empty room echo. Therefore, it is inevitable to apply a clutter reduction process to suppress clutter echoes, and thereby enhance the target (i.e., an individual) echoes.

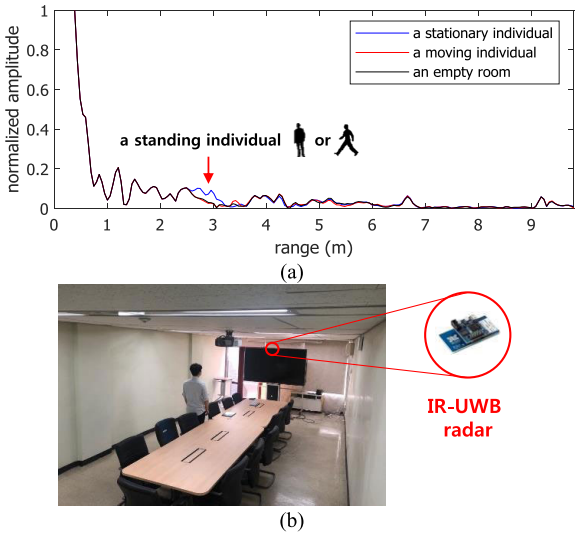

FIGURE 1. (a) Normalized measured echoes in an indoor environment via IR-UWB radar: received signal from a stationary (i.e., standing and stationary) individual (indicated by the blue line), from a moving (i.e., standing and moving) individual (indicated by the red line), and from an empty room with only clutter and without an individual (indicated by the black line). (b) Structure of the room wherein the measured echoes in Fig. 1a were obtained. The IR-UWB radar (indicated by the red circle) with a center frequency of 7.29 GHz and a bandwidth of 1.5 GHz was used. Detailed information of the IR-UWB radar is presented in Section III.A.

If we can estimate the background clutter echoes (which are included in the received signal), a significant portion of clutter echoes can be reduced by subtracting the estimated clutter echoes from the received echoes as follows:

$$\bar{\mathbf{y}}_i = \bar{\mathbf{x}}_i - \bar{\mathbf{x}}_{c,i}, \tag{6}$$

where $\bar{\mathbf{x}}_{c,i}$ is an estimated clutter echo in normalized i^{th} received signal $\bar{\mathbf{x}}_i$. Thus, $\bar{\mathbf{y}}_i$ denotes the clutter-free signals, which will be used later for target detection. The clutter reduction process in (6) is used to maximize $\bar{\mathbf{y}}_i$ at the location of an individual and also to minimize $\bar{\mathbf{y}}_i$ at the location of clutter. To achieve the purpose, the estimate of clutter echo, $\bar{\mathbf{x}}_{c,i}$, should resemble $\bar{\mathbf{x}}_i$ as closely as possible at clutter range bins, whereas $\bar{\mathbf{x}}_{c,i}$ should differ from $\bar{\mathbf{x}}_i$ as much as possible at the range bins of an individual. Base on the above criteria, we investigate and compare following three techniques.

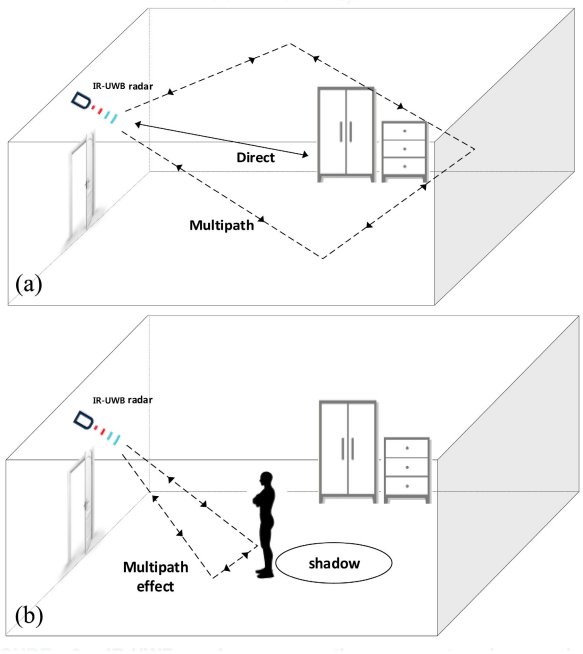

FIGURE 2. IR-UWB radar propagation geometry in an indoor environment. (a) Reflection mechanism in an empty room. (b) Mutual interactions owing to the presence of a standing individual in a reflection mechanism.

The simplest way to estimate clutter echo $\bar{\mathbf{x}}_{c,i}$ is to measure the echoes relative to the empty room with only background clutter and without an individual [5], [34], which is termed as "reference method (RM)" in this paper and is described as follows:

$$\bar{\mathbf{x}}_{c,i} = \frac{1}{n_p}\sum_{k=1}^{n_p}\bar{\mathbf{x}}_k, \quad i = 1, 2, \ldots, \boldsymbol{n_p}, \tag{7}$$

where $\bar{\mathbf{x}}_k$ denotes an empty room echo of each pulse, and thus $\bar{\mathbf{x}}_{c,i}$ denotes the average background clutter echo for the empty room during a single frame consisting of n_p pulses. If the room is empty (i.e., without any individual), then the clutter signal $\bar{\mathbf{x}}_{c,i}$ is updated with the result of (7). Specifically, RM exhibits advantages of low computation complexity, while the performance in terms of clutter reduction is poor especially for a moving individual.

In an empty room (Fig. 2a), the background clutter echo is mainly composed of both the direct reflections from stationary clutter (e.g., furniture, ceiling, floor, and walls) and multiple reflections among the stationary clutter. However, when an individual enters the room, the background clutter echo is highly affected by interactions between an individual and the stationary clutter. The major sources of these interactions consist of two components, namely multiple reflections between an individual and clutter, and shadow effects, as shown in Fig. 2b. It should be noted that the interactions between an individual and clutter are not considered when computing (7). In other words, RM cannot reflect the variation occurred from these interactions because computed $\bar{\mathbf{x}}_{c,i}$ in (7) is not revised after an individual enters the room. Thus, $\bar{\mathbf{y}}_i$ obtained from (6) with RM typically has high amplitude even at the location of clutter, thereby leading to high false alarm rates in later detection results. The phenomenon is especially pronounced for moving individual as opposed to a stationary individual because the mutual interactions severely vary as the individual is moving. These time-varying interactions further degrade the performance of RM.

Another clutter reduction scheme, namely running average filter (RAF) [10], [13] computes clutter echo, $\bar{\mathbf{x}}_{c,i}$, as follows:

$$\bar{\mathbf{x}}_{c,i} = \begin{cases} \dfrac{1}{n_p}\sum_{k=1}^{n_p}\bar{\mathbf{x}}_k, & \text{if } i = 1, \\ \alpha\bar{\mathbf{x}}_{c,i-1} + (1-\alpha)\,\bar{\mathbf{x}}_i, \text{with } 0 < \alpha < 1 & \text{if } i > 1, \end{cases} \tag{8}$$

where $\bar{\mathbf{x}}_i$ denotes the i^{th} received signal and $\bar{\mathbf{x}}_{c,i-1}$ is clutter echo in $(i-1)^{\text{th}}$ received signal. In other words, $\bar{\mathbf{x}}_{c,i}$ in (8) corresponds to the weighted sum of the currently received echo $\bar{\mathbf{x}}_i$ and the previously estimated clutter echo $\bar{\mathbf{x}}_{c,i-1}$. If $i = 1$, $\bar{\mathbf{x}}_{c,i}$ is the same as (7), which means that the initial clutter echo of RAF is identical to the clutter echo computed by RM. In RAF, $\bar{\mathbf{x}}_{c,i}$ is continuously updated at every pulse using the currently received echo $\bar{\mathbf{x}}_i$. Therefore, RAF can consider the pulse-to-pulse variations of clutter echo, and thus the good performance of RAF is expected especially for a moving individual.

As shown in (8), the value of α determines the relative contribution between the previously estimated clutter echo, $\bar{\mathbf{x}}_{c,i-1}$, and currently received echo, $\bar{\mathbf{x}}_i$, in estimating current clutter echo, $\bar{\mathbf{x}}_{c,i}$. It should be noted that the value of α significantly affects the result of clutter reduction. To understand the dependency on the value α against the performance of RAF, we demonstrate the performance of RAF in case of $\alpha \approx 1$ and $\alpha \approx 0$, as examples. By substituting the second equation of (8) into (6), $\bar{\mathbf{y}}_i$ is expressed as follows:

$$\bar{\mathbf{y}}_i = \alpha(\bar{\mathbf{x}}_i - \bar{\mathbf{x}}_{c,i-1}). \tag{9}$$

If α is set relatively close to unity, (8) yields the following expression:

$$\bar{\mathbf{x}}_{c,i} \approx \frac{1}{n_p}\sum_{k=1}^{n_p}\bar{\mathbf{x}}_k \quad for\ \forall i, \tag{10}$$

which is equal to (7). Thus, the clutter-free signal, $\bar{\mathbf{y}}_i$, in (9) can be expressed as follows:

$$\bar{\mathbf{y}}_i \approx \bar{\mathbf{x}}_i - \frac{1}{n_p}\sum_{k=1}^{n_p}\bar{\mathbf{x}}_k. \tag{11}$$

By (11), we expect that RAF with $\alpha \approx 1$ and RM share similar performance in terms of clutter reduction.

On the other hand, if α is set close to zero, (8) yields the following expression

$$\bar{\mathbf{x}}_{c,i} \approx \bar{\mathbf{x}}_i \quad for\ \forall i. \tag{12}$$

Thus, by substituting $\bar{\mathbf{x}}_{i-1}$ for $\bar{\mathbf{x}}_{c,i-1}$ in (9), $\bar{\mathbf{y}}_i$ can be expressed as follows:

$$\bar{\mathbf{y}}_i \approx \alpha(\bar{\mathbf{x}}_i - \bar{\mathbf{x}}_{i-1}). \tag{13}$$

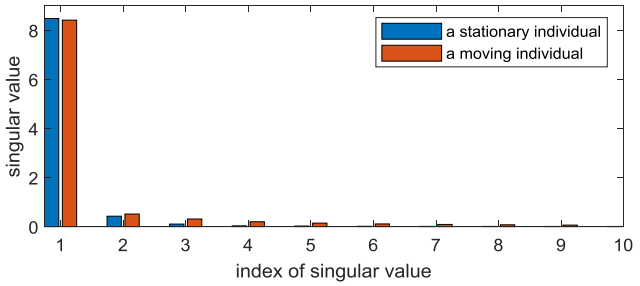

FIGURE 3. Singular values obtained by applying SVD to a normalized matrix, $\overline{\mathbf{X}}$.

(13) denotes that $\overline{\mathbf{y}}_i$ is proportional to the difference of currently received echo, $\overline{\mathbf{x}}_i$ and previously received echo, $\overline{\mathbf{x}}_{i-1}$. Thus, in case of RAF with $\alpha \approx 0$, we expect that $\overline{\mathbf{y}}_i$ has large peaks caused by pulse-to-pulse fluctuations from the motion of a human, whereas $\overline{\mathbf{y}}_i$ has a low amplitude when the object is stationary.

The last scheme for clutter reduction is to use singular value decomposition (SVD) to estimate clutter signals [22], [26], [36]. If we apply SVD to the normalized matrix $\overline{\mathbf{X}}$, consisting of n_p normalized received signals (i.e., $\overline{\mathbf{X}} = [\overline{\mathbf{x}}_1 \overline{\mathbf{x}}_2 \dots \overline{\mathbf{x}}_i \dots \overline{\mathbf{x}}_{n_p}]$), $\overline{\mathbf{X}}$ is factorized as follows:

$$\overline{\mathbf{X}} = \mathbf{U} \sum \mathbf{V}^T, \tag{14}$$

where $(\cdot)^T$ denotes the transpose operation. The matrix $\mathbf{U} = [\mathbf{u}_1 \mathbf{u}_2 \dots \mathbf{u}_{n_r}]$ corresponds to an $n_r \times n_r$ unitary matrix whose columns are termed as left singular vectors. Specifically, $\sum$ is an $n_r \times n_p$ diagonal matrix and its diagonals, σ_k, in descending order for $1 \leq k \leq n_p$, are referred to as singular values. The matrix $\mathbf{V} = [\mathbf{v}_1 \mathbf{v}_2 \dots \mathbf{v}_{n_r}]$ corresponds to an $n_p \times n_p$ unitary matrix whose columns are termed as right singular vectors. Subsequently, with the use of low-rank approximation [37]–[39], $\overline{\mathbf{X}}$ is approximated as $\overline{\mathbf{X}}_r$ with r largest singular values as follows:

$$\overline{\mathbf{X}}_r = \mathbf{U} \sum\nolimits_r \mathbf{V}^T, \tag{15}$$

where $\sum_r$ corresponds to $n_r \times n_p$ diagonal matrix whose diagonals are identical to those of $\sum$ for $1 \leq k \leq r$ and zeros for $r < k \leq n_p$. The desired clutter matrix $\overline{\mathbf{X}}_c = [\overline{\mathbf{x}}_{c,1} \overline{\mathbf{x}}_{c,2} \dots \overline{\mathbf{x}}_{c,i} \dots \overline{\mathbf{x}}_{c,n_p}]$ is obtained via (15), provided that we can select the proper value of r.

To determine the proper value of r, it is important to investigate the singular values in Fig. 3 obtained by applying SVD to the normalized matrix $\overline{\mathbf{X}}$ corresponding to stationary individual and moving individual, respectively. For both stationary and moving individuals, the first singular value, σ_1, significantly exceeds the remaining singular values. As shown in Fig. 1, although an individual exists in the room, it is noted that the received signal $\overline{\mathbf{x}}_i$ is mainly composed of signals from clutter rather than those from an individual. Therefore, the subspace spanned by the first singular value σ_1 and associated left and right singular vectors, $\mathbf{u}_1$ and $\mathbf{v}_1$, is likely to originate from the clutter rather than an individual. Thus, the proper value of r is set to 1 for low-rank approximation in (15), and this leads to the following expression:

$$\overline{\mathbf{X}}_c = \sigma_1 \mathbf{u}_1 \mathbf{v}_1^T. \tag{16}$$

After obtaining $\overline{\mathbf{X}}_c$, the clutter-free signal, $\overline{\mathbf{y}}_i$, as computed using (6), and the clutter-free matrix, $\overline{\mathbf{Y}} = [\overline{\mathbf{y}}_1 \overline{\mathbf{y}}_2 \dots \overline{\mathbf{y}}_i \dots \overline{\mathbf{y}}_{n_p}]$, are established. Consequently, $\overline{\mathbf{X}}_c$ is derived from $\overline{\mathbf{X}}$ which contains already received echoes, including the current one. Thus, the superior performance of SVD is expected for a moving object, same as that of RAF.

Figure 4 shows the clutter-free signal $\overline{\mathbf{y}}_i$ obtained by RM, RAF, and SVD against empty room, the stationary individual at 3 m, and moving individual at around 3 m. Compared to the original received echo in Fig. 1a, a large portion of clutter signals are effectively suppressed by these three methods, thereby increasing the direct reflection from an individual between 2.5 m and 3.3 m and effectively suppressing a significant portion of clutter signals for the range of 0-2.5 m and beyond 3.3 m. However, at ranges beyond 3.3 m, small and perceptible fluctuations still remain due to the interactions, such as multipath and shadow effects, between an individual and stationary clutter. Especially in case of RM (Fig. 4a), the degree of these fluctuations is relatively high compared to that of RAF and SVD. This is because that RM cannot reflect the variation that occurred from these interactions, while both RAF and SVD can reflect these variations in estimating clutter echo.

It should be noted that the relative signal level of the individual and that of clutter (as opposed to the absolute level of the individual) is more important in terms of detection performance. Thus, it is essential to obtain a high signal to clutter ratio (SCR) in clutter-free echo $\overline{\mathbf{y}}_\mathbf{i}$ between individuals and clutter for robust detection performance. The value of SCR of $\overline{\mathbf{y}}_\mathbf{i}$ is also denoted in Fig. 4. They are computed as follows:

$$\mathrm{SCR} = \frac{A^2}{\sigma_C^2}, \tag{17}$$

where A denotes the average amplitude of $\overline{\mathbf{y}}_i$ between 2.5 m and 3.3 m corresponding to direct reflections from an individual in Fig. 4, and σ_C^2 is the average clutter power of $\overline{\mathbf{y}}_i$ outside of ranges between 2.5 m and 3.3 m corresponding to clutter range-bins in Fig. 4.

Based on the observation of $\overline{\mathbf{y}}_i$ and its SCR value indicated in Fig. 4, results of clutter reduction are presented as follows:

- RM yields high SCR, leading to gives good clutter reduction, while the result for a stationary individual, yields low SCR, leading to poor one for a moving individual (Fig. 4a). Because RM is vulnerable to the increased mutual interactions due to a moving individual as previously discussed, the performance of RM for a moving individual is inferior to that for a stationary individual.
- For a stationary individual, RAF with $\alpha = 0.9$ have high SCR values (solid line in Fig. 4b). This result is similar

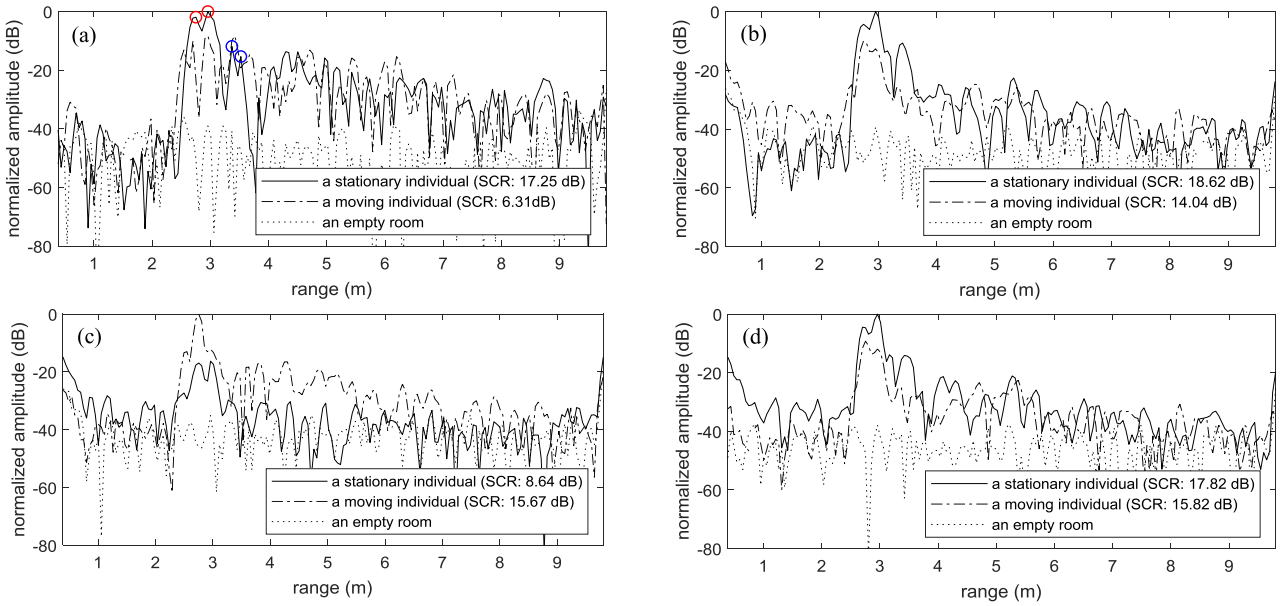

FIGURE 4. Clutter-free signal, $\bar{\mathbf{y}}_i$, of a stationary (i.e., standing and stationary) individual and a moving (i.e., standing and moving) individual at range of 3 m. Note that $\bar{\mathbf{y}}_i$s in Fig. 4 were normalized such that their ranges are between 0 to 1. (a) obtained by RM. Two peaks indicated by red circles are direct reflections from an individual, and ones indicated by blue circles are multiple reflections between the human and the floor. (b) by RAF with $\alpha = 0.9$. (c) by RAF with $\alpha = 0.1$. (d) by SVD.

to that of RM, as expected by (11). Conversely, for a moving individual, RAF with $\alpha = 0.9$ results in higher SCR (dash-dot line in Fig. 4b) than that of RM. This is because RAF, even with $\alpha = 0.9$ in (8), can faithfully reflect the pulse-to-pulse variations of clutter echo in estimating the current clutter echo, $\bar{\mathbf{x}}_{c,i}$. Therefore, for both stationary and moving individual, RAF with $\alpha = 0.9$ leads to good detection performance.

- RAF with $\alpha = 0.1$ yields very low SCR for a stationary individual and yields high SCR for a moving individual, as expected by (14) (Fig. 4c). This implies that RAF with $\alpha = 0.1$ is more advantageous in terms of clutter reduction against the moving individual when compared to that of RM and RAF with $\alpha = 0.9$.
- For both stationary and moving individual, SVD yields high SCR (Fig. 4d). This is because in estimating the clutter echoes, both RAF and SVD can reflect pulse-to-pulse variations, which are caused by the existence of an individual. Hence, for both stationary and moving individual, SVD leads to good detection performance.

In order to obtain the overall conclusions of three techniques (i.e., RM, RAF, and SVD) in terms of clutter reduction, we investigate the average SCR of 144 normalized received signals, $\bar{\mathbf{x}}_i$ ($\mathrm{SCR}_{\bar{\mathbf{x}}_i}$) and clutter-free signals, $\bar{\mathbf{y}}_i$ ($\mathrm{SCR}_{\bar{\mathbf{y}}_i}$) for stationary individual and moving individual, respectively. Additionally, an improvement factor (IF) after the clutter reduction process is computed, as follows:

$$\mathrm{IF} = \mathrm{SCR}_{\bar{\mathbf{y}}_i}(\mathrm{dB}) - \mathrm{SCR}_{\bar{\mathbf{x}}_i}(dB). \tag{18}$$

As previously discussed, the capability of clutter reduction differs between ranges before the individual and those beyond the individual. To clarify it, in Table 1, the average SCR $\bar{\mathbf{x}}_i$, $\mathrm{SCR}_{\bar{\mathbf{y}}_i}$, and IF against different clutter reduction techniques are divided into three sub-tables: ranges between 0 m and 2.5 m (i.e., before the individual), ranges between 3.3 m and 9.4 m (i.e., after the individual), and ranges before and after the individual.

TABLE 1. SCR [dB] of $\bar{\mathbf{x}}_i$, SCR [dB] of $\bar{\mathbf{y}}_i$, and IF [dB].

	Range of 0 m-2.5 m as clutter area					
	Stationary individual			Moving individual		
	$\mathrm{SCR}_{\bar{\mathbf{x}}_i}$	$\mathrm{SCR}_{\bar{\mathbf{y}}_i}$	IF	$\mathrm{SCR}_{\bar{\mathbf{x}}_i}$	$\mathrm{SCR}_{\bar{\mathbf{y}}_i}$	IF
RM	-2.65	37.08	39.73	-5.16	28.41	33.57
RAF (α=0.1)	-2.65	15.33	17.98	-5.16	28.19	33.35
RAF (α=0.5)	-2.65	20.83	23.48	-5.16	28.91	34.07
RAF (α=0.9)	-2.65	31.06	33.71	-5.16	30.02	35.18
RAF (α=0.99)	-2.65	36.44	39.09	-5.16	29.29	34.45
SVD	-2.65	28.76	31.41	-5.16	28.71	33.87
	Range of 3.3 m-9.4 m as clutter area					
	Stationary individual			Moving individual		
	$\mathrm{SCR}_{\bar{\mathbf{x}}_i}$	$\mathrm{SCR}_{\bar{\mathbf{y}}_i}$	IF	$\mathrm{SCR}_{\bar{\mathbf{x}}_i}$	$\mathrm{SCR}_{\bar{\mathbf{y}}_i}$	IF
RM	7.50	15.83	8.33	4.89	9.99	5.10
RAF (α=0.1)	7.50	13.41	5.91	4.89	15.33	10.44
RAF (α=0.5)	7.50	15.71	8.21	4.89	15.15	10.26
RAF (α=0.9)	7.50	17.17	9.67	4.89	14.32	9.43
RAF (α=0.99)	7.50	16.94	9.44	4.89	13.10	8.21
SVD	7.50	17.07	9.57	4.89	14.29	9.40
	Range of 0 m-2.5 m and 3.3 m-9.4 m as clutter area					
	Stationary individual			Moving individual		
	$\mathrm{SCR}_{\bar{\mathbf{x}}_i}$	$\mathrm{SCR}_{\bar{\mathbf{y}}_i}$	IF	$\mathrm{SCR}_{\bar{\mathbf{x}}_i}$	$\mathrm{SCR}_{\bar{\mathbf{y}}_i}$	IF
RM	-6.28	17.06	23.34	-8.80	11.23	20.03
RAF (α=0.1)	-6.28	12.51	18.79	-8.80	16.14	24.94
RAF (α=0.5)	-6.28	15.48	21.76	-8.80	16.07	24.87
RAF (α=0.9)	-6.28	17.98	24.26	-8.80	15.41	24.21
RAF (α=0.99)	-6.28	18.09	24.37	-8.80	14.23	23.03
SVD	-6.28	17.53	23.81	-8.80	15.38	24.18

The first sub-table in Table 1 presents the clutter reduction performance when the received echo is mainly composed of direct reflections from the individual and clutter, without any higher-order interactions such as multipath and

shadow effects. In the first sub-table, RM and SVD yield high IF values, i.e., they achieve a good clutter reduction performance, whether the individual is stationary or not; this is due to the significantly few higher-order interactions between the individual and clutter in the received echo. In the case of RAF with a stationary individual, its performance is primarily influenced by the choice of α. For $\alpha \approx 0$, clutter-free signals $\overline{\mathbf{y}}_i$ have considerably low amplitudes at all ranges, according to (14); this simultaneously leads to low $\mathrm{SCR}_{\overline{\mathbf{y}}_i}$ and IF values. In contrast, the performance of RAF with $\alpha \approx 1$ is similar to that of RM, as shown in (11), resulting in high IF values. In the case of RAF with a moving individual, RAF has high IF values regardless of α, owing to the advantage of RAF for the pulse-to-pulse fluctuations from the moving individual, particularly for $\alpha \approx 0$, as previously discussed.

In the second sub-table of Table 1, the overall IF values are significantly lower than those in the first sub-table because higher-order interactions such as multipath and shadow effects are dominant in the received echoes. Especially, these higher-order interactions lead to poor results in case of RM with a moving individual. The performance of RAF is similar to those in the first sub-table in Table 1, implying that the results depend on the value of α. SVD yields relatively high or similar IF values compared to those of RM or RAF.

The last sub-table in Table 1 depicts the overall clutter reduction results computed at ranges before and after the individual. It is easily noticed that all IF of the three techniques are relatively high whether the individual is stationary or moving. The RM is efficient only for a stationary individual, while RAF with $\alpha = 0.9$ and SVD are efficient for both stationary and moving individual. In the case of RAF, its performance is heavily dependent on the choice of α, particularly for a stationary individual. In a practical situation, the optimum selection of α for RAF is a very difficult task. We summarize the above results and adopt the SVD technique for clutter reduction. According to many additional experiments, we found that the above comparisons about RM, RAF, and SVD based on the results in Table 1, were also valid even for various scenarios, such as the same individual at different ranges (3 m, 5 m, and 7 m), different indoor environments, and different individuals.

3) DETECTION

Subsequently, CFAR detector was applied to each clutter-free signal, $\overline{\mathbf{y}}_i$, to detect a standing individual. CFAR detector is generally referred to as 'adaptive threshold detection', implying that the threshold of the detector is automatically adjusted according to the power of adjacent area of the target to maintain 'constant false alarm rate' [40]. There are many different versions of CFAR detectors, and thus, we considered four kinds of CFAR detectors: cell averaging CFAR (CA-CFAR) detector, greatest of cell-averaging CFAR (GOCA-CFAR) detector, smallest of cell-averaging CFAR (SOCA-CFAR) detector, order-statistics CFAR (OS-CFAR) detector. The basic form of CFAR detector is CA-CFAR

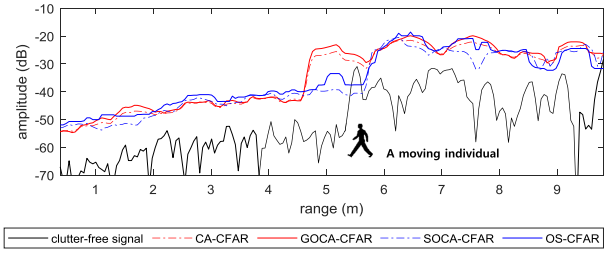

FIGURE 5. Clutter-free signal denoting a moving individual (with walking motion) at 5.5 m and four CFAR thresholds.

algorithm, and its threshold T is computed as follows:

$$T = N_{ref}(p_{fa}^{1/N_{ref}} - 1)\hat{\beta}^2 \tag{19}$$

where N_{ref} denotes the number of reference cells, p_{fa} denotes the false alarm rate, and $\hat{\beta}^2$ denotes the average power of reference cells. As shown in (19), the threshold of CA-CFAR algorithm is proportional to the average power of reference cells. In case of the other three CFAR detectors, their thresholds are computed using larger power of reference cells (GOCA-CFAR) between two reference windows or smaller one (SOCA-CFAR) or median value among the powers of all reference cells (OS-CFAR).

Figure 5 shows the clutter-free signal and thresholds obtained by applying various CFAR techniques to $\overline{\mathbf{y}}_i$. False alarm rate (p_{fa}) is set to 10^{-6}, the number of reference cells (N_{ref}) is 20, and the number of guard cells (N_{guard}) is 20. Note that the physical length of one range-bin is nearly 0.05 m. Even after clutter reduction, $\overline{\mathbf{y}}_i$ still exhibits slightly large multiple reflections (at ranges between 6 m to 7.5 m in the black-line of Fig. 5), which mainly comes from the walking motions. When computing the threshold of CA-CFAR, the large multiple reflections tend to raise the threshold and eventually lead to a missed detection. GOCA-CFAR also miss the individual at 5.5 m, because GOCA-CFAR computes the threshold using larger average power. On the other hand, both order-statistics CFAR (OS-CFAR) and SOCA-CFAR can detect the individual at 5.5 m given their capability of detecting the target in non-homogeneous clutter. Thus, in the study, we chose the SOCA-CFAR to detect a standing individual.

C. DETECTION OF AN INDIVIDUAL LYING DOWN

The overall process for detecting an individual lying down also consists of two processes, namely clutter reduction and detection, same as those of standing individual. First, it is necessary to efficiently suppress clutter signals in advance. Because signal components from an individual lying down caused by his/her RCS and body motion are very weak in the received echoes, clutter reduction technique should be chosen in accordance with an accurate analysis. In a majority of the cases, the individual lying down is almost stationary and has considerably low RCS (as shown in Fig. 6a). Furthermore, significantly few multipath and shadow effects were observed between the individual lying down and clutter. Hence, based

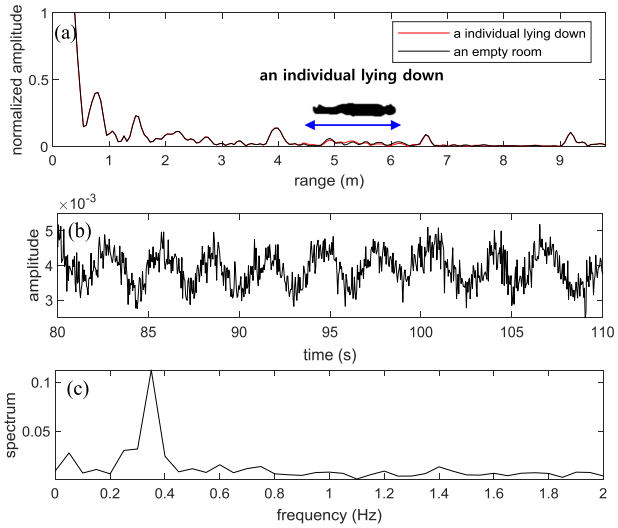

FIGURE 6. (a) Normalized measured echoes from an individual lying down (the red line) and those from the empty room (the black line). (b) Time-series at a range bin of an individual lying down (i.e., being located at 5 m from the radar in Fig. 6a), and (c) its frequency spectrum.

on the results in the first sub-table of Table 1, the RM technique is employed for clutter reduction to detect the individual lying down. In the same manner of investigating the performance of clutter reduction for a standing individual, we carried out some experiments to obtain IF in (18) using the received echo from an individual lying down (the red line in Fig. 6). As expected, RM gives the highest value of IF = 30.25, RAF with $\alpha = 0.9$ gives 24.05, RAF with $\alpha = 0.1$ gives 15.14, and SVD IF = 20.28. It means that RM is superior to RAF and SVD in terms of clutter reduction for an individual lying down having very low RCS. Hence, RM was used in the study to remove clutter signal for detection of an individual lying down.

Even though the RM can reduce the clutter component to the minimum possible level, the conventional CFAR technique for detecting a standing individual can produce poor detection results in the case of an individual lying down. Because RM cannot completely remove clutter components in received echo due to slight variations in the clutter environment or time-varying characteristics of a radar system, it is likely that the detection of an individual lying down is not perfect in the range domain. Thus, for detecting an individual lying down, we devise a two-stage detection process, namely detection in the range domain and detection of respiratory movement in the frequency domain.

In the first detection stage, we applied a CA-CFAR detector with high false alarm rate to the clutter-free signal in the range domain, and this ensures a high detection probability of the individual lying down. After the first stage, the miss-detection probability of the individual lying down is minimized, but many range bins with clutter only can be detected, leading to a high false alarm rate. The high false alarm probability in the first stage can be significantly reduced via the detection of the respiratory movement of the individual lying down in the second stage, which can be effectively accomplished in the frequency domain.

In the second detection stage, we also applied the CA-CFAR detector with low false alarm rate to frequency spectra of time-series obtained by Fourier transform (FT) at all detected range bins in the first stage. The time-series corresponding to the individual lying down is shown in Fig. 6b, which shows a clear periodic signal generated by respiratory movement. The periodic signal causes a peak at 0.35 Hz in the frequency domain, i.e., respiration rate in the frequency domain as shown in Fig. 6c. Generally, it is well known that the respiration rate of a human occurs between 0.2 Hz (12 breaths per minute) and 0.3 Hz (18 breaths per minute) [41]. Given this fact, we applied the CA-CFAR threshold to all frequency bins between 0.1 Hz and 0.5 Hz with a low false alarm rate. The CA-CFAR threshold in the frequency domain is also computed by (19) with the low false alarm rate. The reference cells are fixed and selected as N_{ref} frequency bins beyond 10 Hz, because the frequency range for human motion is typically less than 10 Hz [42]. After applying the CA-CFAR threshold to all frequency spectra corresponding to range bins detected in the first stage, we finally make a decision of the presence of an individual lying down. In other words, if more than one spectra exceed the CA-CFAR threshold, the existence of an individual lying down is declared.

Figure 7 shows the result of a two-stage detection process applied to a clutter-free echo, which contains the reflection from an individual lying down. Figure 7a shows the clutter-free echo (the black line) and CA-CFAR threshold (the red line) with a high false alarm rate (10^{-1}) in the range domain. Many range bins corresponding to various parts of the human body are detected, and a false alarm at 2.5 m is detected. For example, Figures 7b – d show the frequency spectrum at 42^{nd}(false alarm), 95^{th}, and 102^{nd} (human body) range bins, respectively. As shown in Fig. 7b, the frequency spectrum with clutter only between 0.1 Hz and 0.5 Hz does not exceed the CA-CFAR threshold with the low false alarm rate (10^{-12}), while those (Fig. 7c and 7d) of the human body exceed the threshold. In the frequency domain, the false alarm at the 42^{nd} range bin can be rejected, thereby resulting in lowering the false alarm rate. Therefore, as a result, the human body lying down is detected without any false alarms, declaring the presence of an individual. Note that the individual lying down lets his/her body stationary as much as possible not to be detected by his/her body motion. The individual lying down in all experiments of this paper follows this rule.

On the other hand, Fig. 8 shows detection outcomes for the case of an empty room with clutter only. As mentioned before, RM cannot completely remove stationary clutter, and thus several large peaks are detected in the range domain (Fig. 8a) even for an empty room. However, any detected bin in the range domain does not exceed the CA-CFAR threshold in the frequency domain as shown in Fig. 8b – d. Hence, in the second detection stage, we can declare that the room is empty.

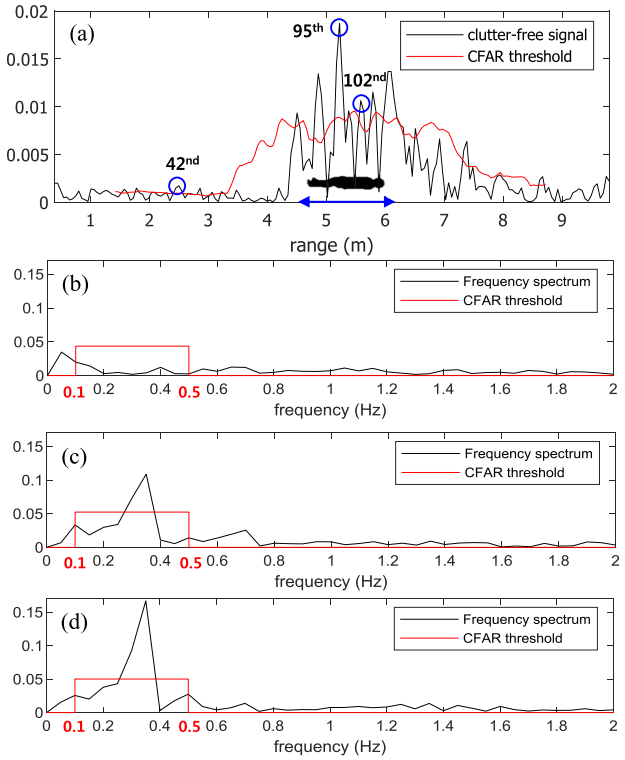

FIGURE 7. Two-stage detection against the measured echo from an individual lying down. (a) The clutter-free signal (the black line) that contains the component from an individual lying down and CA-CFAR detector (the red line) with false alarm of 10^{-1} and the number of reference cells (N_{ref}) is 20, and the number of guard cells (N_{guard}) is 20. (b) The frequency spectrum obtained by time series of 42nd range-bin (the black line), which is one of the detected range bins in Fig. 7a and CA-CFAR threshold (the red line) with false alarm of 10^{-12} and N_{ref} of 20, computed by (19). (c) and (d) are frequency spectrum (black lines) and CA-CFAR threshold (red lines) corresponding to the 95th range bin and 102nd range bin, respectively.

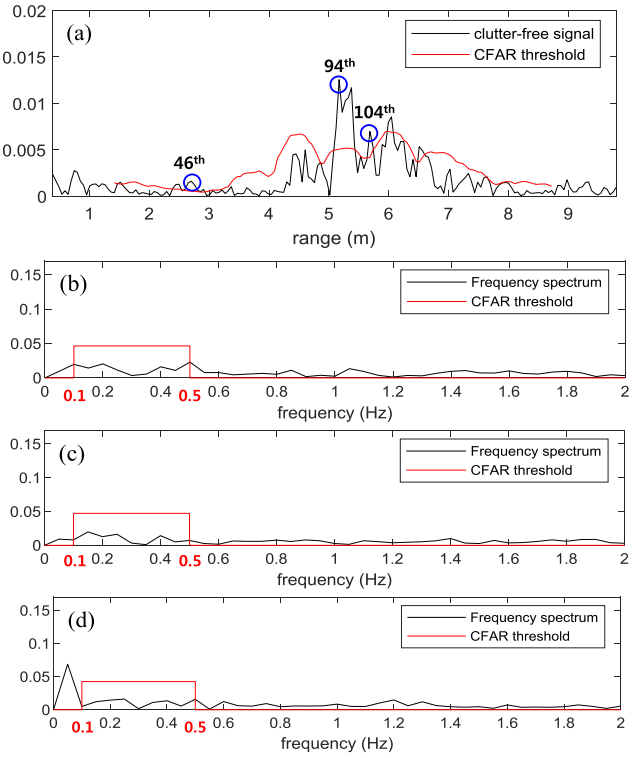

FIGURE 8. Two-stage detection against the measured echo from the empty room. (a) The clutter-free signal (the black line) that contains only clutter and CA-CFAR detector (the red line) with false alarm of10^{-1} and the number of reference cells (N_{ref}) is 20, and the number of guard cells (N_{guard}) is 20. (b) The frequency spectrum obtained by time series of 46th range-bin (the black line), which is one of the detected range bins in Fig. 8a and CA-CFAR threshold (the red line) with false alarm of 10^{-12} and N_{ref} of 20, computed by (19). (c) and (d) are frequency spectrum (black lines) and CA-CFAR threshold (red lines) corresponding to 94th range bin and 104th range bin, respectively.

We summarize the two-stage detection for an individual lying down as follows:

A. Detect range bins using CA-CFAR detector with high false alarm rate.
B. Obtain all frequency spectra at range bins detected in part A.
C. Apply CA-CFAR threshold with low false alarm rate to all frequency spectra between 0.1 Hz and 0.5 Hz.
D. At least, if one of them exceeds the CA-CFAR threshold, then declare the existence of an individual.

D. ALGORITHM SUMMARY

The flowchart of the overall detection scheme (Fig. 9) for the presence of individuals in a room is a sequential combination of detection of a standing individual (Step 1 in Fig. 9) and that of an individual lying down (Step 2 in Fig. 9). First, the detection of a standing individual (Step 1.A and B) is performed as

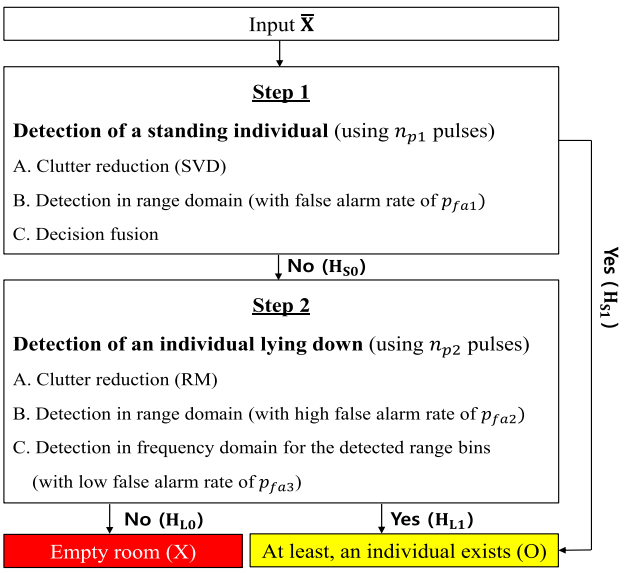

FIGURE 9. Flowchart of the proposed detection scheme.

discussed in Section II.B. It is noted that the detection scheme for a standing individual is applied to n_{p1} pulses consisting of a single frame, $\overline{\mathbf{X}}$, and detection outcomes obtained from

n_{p1} pulses (i.e., total n_{p1} outcomes) are collected. Finally, the presence of a standing individual is determined based on decision fusion (Step 1.C) by using n_{p1} detection outcomes as follows:

$$\begin{cases} \mathrm{H_{S0}}: \text{A standing individual does not exist,} \\ \qquad \textit{if } \eta = n_d/n_{p1} < 50\% \\ \mathrm{H_{S1}}: \text{A standing individual exists, } \textit{if } \eta \geq 50\% \end{cases} \tag{20}$$

where n_d denotes the number of pulses whose outcomes support the existence of a standing individual. When the detection scheme described in Section II.B is exploited for several pulses, the detection outcomes may differ from each other due to severe RCS fluctuations especially for a moving individual, thereby resulting in some missed detections. Conversely, some false alarms can be observed even for the empty room because of the imperfect clutter cancellations. To overcome the limitations, we adopted the decision fusion strategy in (20).

If $\mathrm{H_{S1}}$ is declared as a result of (20) (i.e., a standing individual exists), the overall detection scheme directly produces the final result as the existence of an individual (i.e., O). Otherwise, in the case of $\mathrm{H_{S0}}$, a further step of detection of an individual lying down in Section II.C (Step 2 in Fig. 9) should be performed to declare $\mathrm{H_{L1}}$ or $\mathrm{H_{L0}}$. It should be noted that the detection outcome for an individual lying down is obtained using n_{p2} pulses, which typically exceeds that of standing individual, n_{p1}. In order to detect the respiratory movement (which is very weak and slow), the two-stage detection in Section II.C needs sufficient observation time to obtain fine-resolution in the frequency domain. The observation time is directly proportional to the number of pulses, and thus $n_{p1} < n_{p2}$ in most cases.

Consequently, if an individual lying down is present (i.e., $\mathrm{H_{S0}}$ and $\mathrm{H_{L1}}$), the overall detection scheme declares the existence of an individual (i.e., O). Otherwise (i.e., $\mathrm{H_{S0}}$ and $\mathrm{H_{L0}}$), an empty room is declared (i.e., X).

III. EXPERIMENTAL RESULTS

In this section, we assess the performance of the proposed detection scheme for the presence of individuals under indoor and daily life situations.

A. EXPERIMENTAL SETUP

The detection experiments were performed using IR-UWB radar, i.e., single-chip radar sensor with XeThru module X4M03 developed by Novelda. The specification of the IR-UWB radar used in the experiments is as follows:

- Center frequency: 7.29 GHz
- Bandwidth: 1.5 GHz (range resolution: 0.1 m)
- Pulse repetition frequency (PRF): 24 Hz
- Maximum detection range: 9.87 m
- Number of range bins, n_r: 184 bins

In Table 2, the parameter setup for the proposed detection scheme is summarized. As 24 pulses are used for Step 1, which is depicted in Fig. 9, with a PRF of 24 Hz, the proposed method determines the presence of an individual at every second. In the case of $\mathrm{H_{S0}}$ (i.e., a standing individual does not exist) in (20), Step 2, requires 240 pulses (for ensuring sufficient frequency resolution) to decide the presence of an individual lying down. This implies that Step 2 requires an additional 10 s to reach a decision. Thus, during this additional 10 s, the proposed method retains the previous final outcomes. After Step 2 has been completed, the final outcome is updated based on the results of Steps 1 and 2. Note that we set probabilities of false alarms p_{fa1}, p_{fa2}, and p_{fa3}, for CFAR detectors of the proposed method as the same values in all detection experiments (from Fig. 11 to Fig. 15) with different indoor environments.

TABLE 2. Parameter setup.

Step 1	The number of pulses used for the detection of a standing individual	n_{p1}	24
	The probability of false alarm rate for CFAR detection in the range domain	p_{fa1}	10^{-6}
Step 2	The number of pulses used for the detection of an individual lying down	n_{p2}	240
	The probability of false alarm rate for CFAR detection in the range domain	p_{fa2}	10^{-1}
	The probability of false alarm rate for CFAR detection in the frequency domain	p_{fa3}	10^{-12}

(a) room with normal clutter. (b) room with heavy clutter.

FIGURE 10. Indoor environments where our experiments conducted under. IR-UWB radar (indicated by red circles) placed at a height of 2 m.

Our experiments were conducted in two different types of indoor environments, namely a room (4.5 m × 9.5 m) with one TV, a few tables and chairs (normal clutter environment, see Fig. 10a); and a room (4.5 m × 9.5 m) with a TV, several tables, chairs, books, home appliances and so on (heavy clutter environment, see Fig. 10b). It should be noted that the IR-UWB radar is placed at a height of 2 m (near the ceiling and the inner wall) and the antenna is aligned slightly downward to cover the maximum possible room area. It may be advantageous to install the radar on the ceiling such that its antenna points directly downwards, for detecting an individual lying down. However, the position of the radar shown in Fig. 10 is more beneficial for covering the entire space.

B. STANDING INDIVIDUAL IN A NORMAL CLUTTER ENVIRONMENT

First, we measured echo signals for a standing individual in a normal clutter environment in Fig. 10a. The individual entered the room and walked around a table. Subsequently,

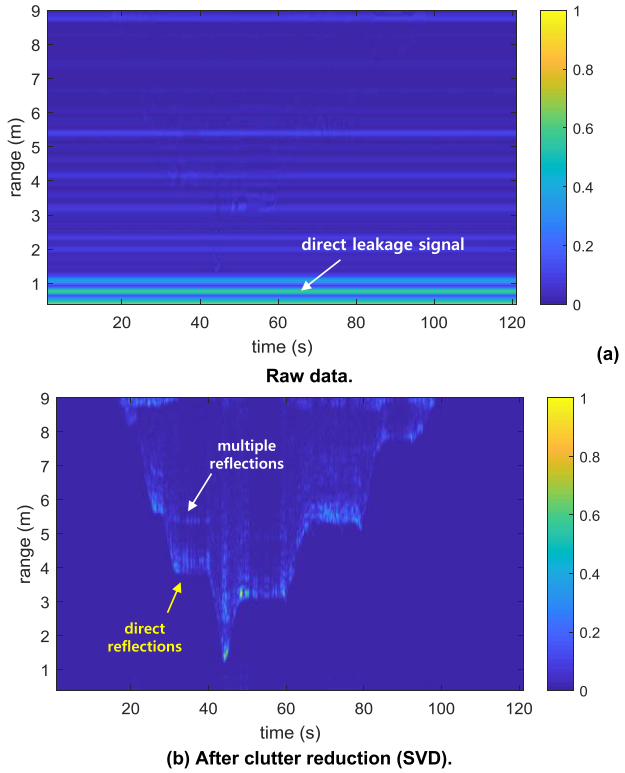

FIGURE 11. Raw data obtained from the experiment with a standing individual in normal clutter (a) and its clutter-suppressed data (b).

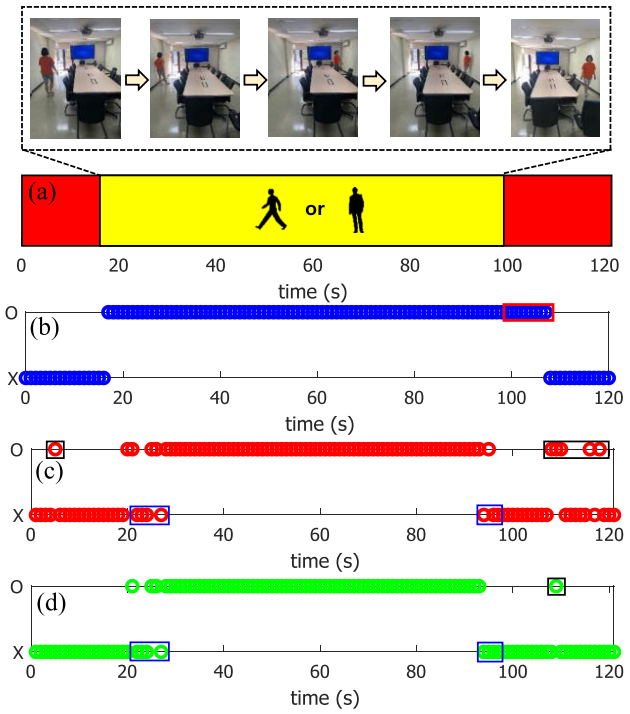

FIGURE 12. Detection result of the standing individual in normal clutter. (a) Ground truth and several pictures showing a standing (stationary or moving) individual. (b) Detection outcome of the proposed detection scheme. 'O' means that 'at least, an individual exists' and 'X' 'empty room'. The red box shows the delay caused by Step 2 in Fig. 9. (c) Detection outcome of conventional range-Doppler processing without any clutter reduction method. Blue boxes denote several missed detections, and black boxes denote several false alarms. (d) Detection outcome of the conventional range-Doppler processing with clutter reduction scheme (SVD). Blue boxes denote missed detection and black boxes denote false alarm.

she left the room. During her stay in the room, she stopped several times. The normalized raw data from the standing individual is shown in Fig. 11a. It is difficult to discriminate the reflections from the individual because they are very weak when compared to the direct leakage signal at 0 m (white arrow in Fig. 11a) from transmitting to receiving antenna and other clutter signals.

After clutter reduction via SVD (Fig. 11b), most of the stationary clutter components decreased, and thus reflections from the standing individual can be enhanced. The reflections from the standing individual were mainly composed of two components: direct reflections and multiple ones. The former is generally caused by the standing individual only. On the other hand, the latter is mainly caused by interactions between the individual and clutter, i.e., multipath effects and shadow (see Fig. 2b) at the range bins behind the individual. For example, between 30 s and 40 s, direct reflections appear at 4 m due to the standing individual (yellow arrow in Fig. 11b) and strong multiple reflections at 5.4 m due to interactions between the individual and ceiling/floor of the room (white arrow in Fig. 11b).

Figure 12 shows the detection outcomes of the proposed method and the conventional range-Doppler processing, which is one of the coherent integration techniques enabling us to improve the signal to noise ratio (SNR). The range-Doppler map was obtained by using the normalized data $\overline{\mathbf{X}}$ in (5) with the coherent processing interval, $n_{p1} = 24$, which is same as the proposed method. Note that no clutter reduction process was performed. Subsequently, a two-dimensional (2D) CA-CFAR technique with a false alarm rate of 10^{-6} (equal to that of Step 1.B in the proposed method) is applied to each range-Doppler map. If one or more range-Doppler cells have been detected, we declare at least, "O: an individual exists." Otherwise, an "X: empty room" is declared.

When compared to ground truth (Fig. 12a), the outcome of the proposed method (Fig. 12b) exhibits a good agreement with the ground truth with the exception of the results between 97 s and 107 s (red box in Fig. 12b). It is noted that the proposed method requires an observation time to reach a decision on the presence of an individual lying down as discussed in Section II.D. During this time, the proposed method maintains the previous outcome even though the ground truth corresponds to the empty room. Thus, in the interval, 97 s – 107 s, the proposed method keeps the value at 96 s.

By investigating the ground truth (Fig. 12a) and the result of the conventional method (Fig. 12c and Fig. 12d), the outcomes of conventional range-Doppler map processing are similar to the ground truth. However, many false alarms when the outcome is "O" for cases where the room is actually empty (as denoted by black boxes in Fig. 12c and Fig. 12d),

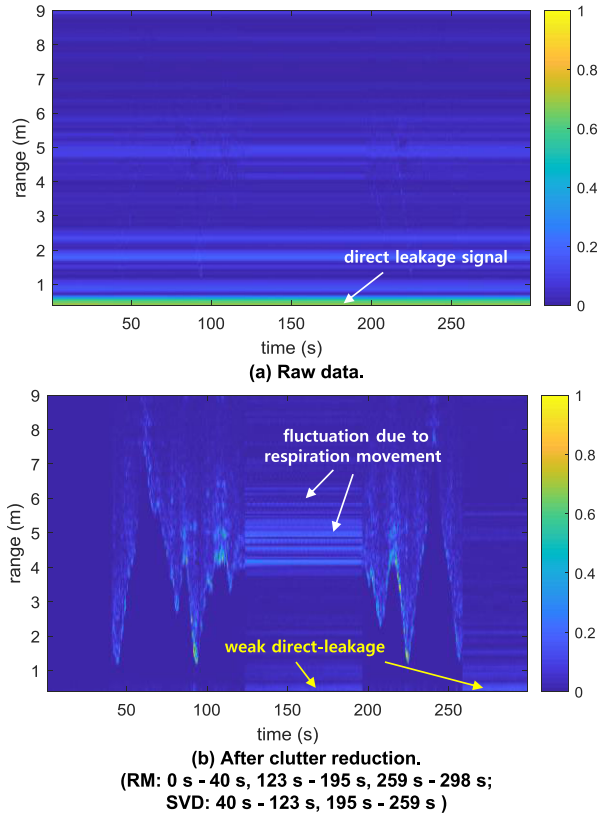

FIGURE 13. Raw data obtained from the experiment with a standing individual or an individual lying down in heavy clutter (a) and its clutter-suppressed data (b).

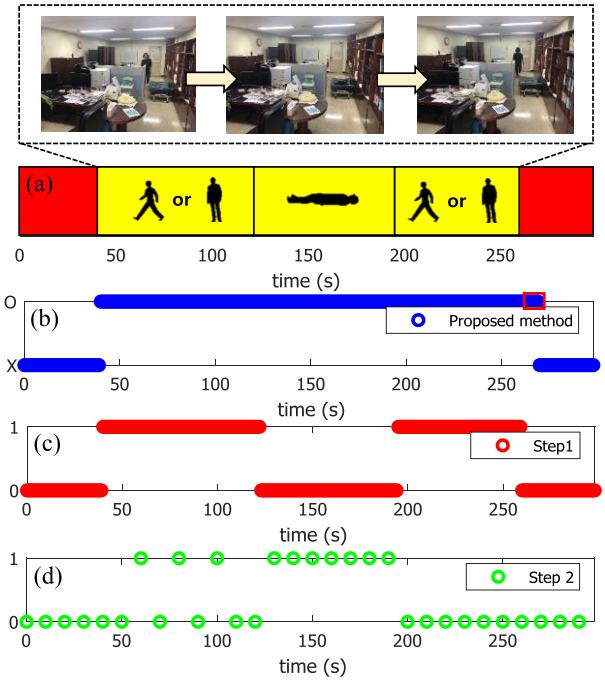

FIGURE 14. Detection result of the standing/lying down individual. (a) Ground truth and several pictures showing a standing/lying down individual. (b) Detection outcome of the proposed detection scheme. 'O' means that 'at least, an individual exists' and 'X' 'empty room'. The red box shows the delay caused by Step 2 in Fig.9. (c) Detection outcome of Step 1 only, ('1': when a standing individual exists; '0': for an individual lying down and for an empty room) and (d) detection outcome of Step 2 only ('1': when an individual lying down exists; '0': for an empty room and for a standing individual).

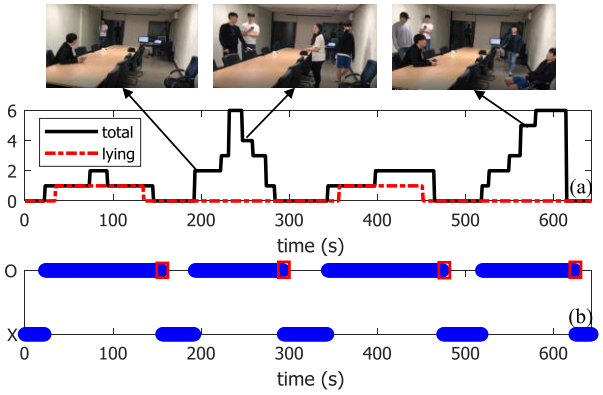

FIGURE 15. Detection result of the mixed situation. (a) Ground truth (vertical axis denotes the number of individuals. 'total' denotes the number of total individuals in the room; 'lying' denotes the number of an individual lying down in the room). (b) Detection outcome of the proposed detection scheme. Red boxes denote the delay caused by Step 2 in Fig.9.

and missed detections when the outcome is "X" despite the existence of an individual in the room are observed (as denoted by blue boxes in Fig. 12c and Fig. 12d). Fig. 12c is the result of range-Doppler processing by using normalized data without any clutter reduction scheme, and Fig. 12d is that of range-Doppler processing coupled with clutter reduction method of SVD. False alarms are mainly caused by clutter components in range-Doppler maps. Thus, most of false alarms can be rejected by applying clutter reduction. However, it is not a satisfactory result compared to that of the proposed method. It is evident that a majority of the missed detections occur when the individual is far from the radar, due to the low SNR. Hence, the proposed method is more robust than conventional range-Doppler processing, in terms of the probability for missed detection and false alarm.

C. INDIVIDUAL LYING DOWN IN A HEAVY CLUTTER ENVIRONMENT

We conducted the experiment for a standing/lying down individual in a heavy clutter environment. The individual entered the room and walked around a table. Thereafter, she lay on the camp bed. After a minute, she stood up and walked around a table again. Subsequently, she left the room. Thus, as shown in Fig. 9, two different methods, SVD for a standing individual (Step 1.A) and RM for an individual lying down (Step 2.A) were utilized to reduce the clutter components contained in the raw data (Fig. 13a), and the result of clutter reduction is shown in Fig. 13b.

In Fig. 13b, when compared to raw data in Fig. 13a, responses due to an individual are pronounced, while those due to clutter are significantly reduced. Specifically, Fig. 13b

exhibits slight RCS fluctuations between 123 s and 195 s (white arrows in Fig. 13b), which are caused by respiratory movement from an individual lying down. However, weak direct-leakage signal from transmitter to receiver and weak clutter signal due to imperfect clutter cancellation of RM are observed between 123 s and 195 s and after 259 s (yellow arrows in Fig. 13b).

Despite the imperfect clutter reduction, our proposed method can accurately predict the presence of the individual whether she was standing or lying down (Fig. 14a and 14b). It is worthy of observing final detection outcomes after the individual leaves the room at 259 s. The ground truth after 259 s is ''empty room.'' However, several weak clutter components still remain in the range domain, and these may result in some false alarms in Step 2.B. Nevertheless, in Step 2.C, through the processing of 240 pulses in the frequency domain during a 10 s period, we can determine that respiratory movements of an individual lying down do not exist, thereby rejecting false alarms in the range domain. Between 259 s and 269 s, the proposed method maintains the previous decision outcome at 258 s (as denoted by the red box in Fig. 14b). The final outcome is reflected at 270 s. Consequently, the proposed method provides the final decision outcome of ''empty room'' at 270 s.

In order to facilitate the understanding of the proposed method, we applied Step 1 only (Fig. 9) to raw data in Fig. 13a, resulting in Fig. 14c. The outcomes using 'Step 1 only' (Fig. 14c) are exactly in agreement with the ground truth against a standing individual (Fig. 14a). It means that the outcomes correspond to '1' only when a standing individual exists and to '0' for an individual lying down and for an empty room.

On the other hand, the outcomes using Step 2 only (Fig. 14d) slightly differ with the ground truth against an individual lying down (Fig. 14a). If Step 2 is only applied to raw data, we expect that the outcomes correspond to '1' only when an individual lying down exists, and corresponds to '0' for an empty room and for a standing individual. However, as a result of Fig. 14d, the outcomes at 60 s, 80 s, and 100 s correspond to '1' for a standing individual. Even though Step 2 was originally designed to detect the individual lying down, it provides an outcome of '1' several times for the standing individual. This is because the respiration motion of a standing individual can also be detected via Step 2. Note that in Table 2, 240 pulses were used to detect an individual lying down and PRF corresponded to 24 Hz. Thus, Step 2 makes a decision every 10 s.

The final outcomes of the proposed method in Fig. 14b differ from outcomes computed by the logical sum of Fig. 14c and 14d, because Step 2 is dependent on Step 1 in the overall algorithm (see Fig. 9). Consequently, the overall detection algorithm in Fig. 9 exhibits good agreement with the ground truth except for a slight delay in Step 2, and this is caused by the time required to ensure a resolution in the frequency domain.

D. MANY INDIVIDUALS IN A NORMAL CLUTTER

Finally, the proposed method was verified by conducting experiments with six individuals in normal clutter. The scenarios depict the real situation, and this is likely to occur in daily life. When some/all the individuals entered the room, they walked or sat on a chair. Sometimes, one of them who entered the room lay on the camp bed. The ground truths are shown in Fig. 15a and the corresponding detection outcomes are shown in Fig. 15b.

As expected, the final outcomes correspond to 'O' when the room is occupied by an individual either standing or lying down and correspond to 'X' for an empty room. When many individuals were standing (from 193 s to 273 s in Fig 15), the proposed method adopted a correct decision, 'O'.

We further performed experiments for the mixed situation (from 74 s to 93 s or from 398 s to 464 s in Fig. 15): individuals entered the room, some individuals were standing, and one of them lay on the camp bed. When at least one individual is standing, the proposed method produces the outcome 'O' because Step 1 confirmed 'H_{S1}' (see Fig. 9). Therefore, the final decision corresponds to 'O' irrespective of the presence of an individual lying down. After all the standing individuals left the room, Step 2 can affect the final decision. For example, at 93 s, a standing individual left the room, and an individual lying down still existed in the room. Thus, the outcome of Step 1 corresponds to 'H_{S0}' while the outcome of Step 2 corresponds to 'H_{L1}', thereby leading to an overall outcome, 'O'.

On the other hand, at 464 s, a standing individual and an individual lying down left the room together. Thus, Step 1 corresponds to 'H_{S0}' and Step 2 also corresponds to 'H_{L0}', thereby leading to the final decision, 'X', after 474 s. It is noted that even if a standing individual left at 463 s, step 2 needs 10 s to reach a final decision, and thus the proposed method maintains the previous outcome until 474 s. Similarly, at 145 s, 283 s, 464 s, and 614 s, 10 s differences between the final decision and ground truth are observed as shown in Fig. 15b (denoted by red boxes). However, with the exception of the 10 s differences between the final decision and ground truth, the proposed detection algorithm can make correct decisions related to presence of individuals for a realistic situation in daily life.

IV. CONCLUSION

This paper presents a robust method to detect the presence of individuals by exploiting IR-UWB radar in an indoor environment. In order to devise detection scheme, we first investigate various clutter reduction techniques to determine an optimal method in terms of detecting a standing individual and an individual lying down, respectively. Thus, SVD was selected as a clutter reduction method for detecting standing individuals as it is efficient to detect both moving and stationary target. For an individual lying down, RM was selected due to its advantages for stationary and low RCS targets. After the clutter reduction, CFAR detection was utilized to detect both

standing and lying down individual lying down. Specifically, in the case of detecting an individual lying down, we adopt two-stage detection: detection in the range domain with high detection probability (i.e., high false alarm rate) and detection of a peak in the frequency domain, which originates from respiratory movement. The processes overcame the imperfect cancellation of clutter component and resulted in the detection of targets with very low RCS. Finally, we validated the proposed detection scheme by conducting experiments under various indoor environments. Results indicated that the proposed method provided robust detection performances even for a heavy clutter environment or realistic situation in daily life.

- Improvement of performance in a harsher condition such as time-varying clutter environment caused by moving objects.
- Validation of detection accuracy for the situation with two or more individuals lying down.

ACKNOWLEDGMENT

Authors would like to express an appreciation for Samsung Electronics for providing IR-UWB radar sensors and measured data.

REFERENCES

[1] M. Z. Win, D. Dardari, A. F. Molisch, W. Wiesbeck, and J. Zhang, "History and applications of UWB," *Proc. IEEE*, vol. 97, no. 2, pp. 198–204, Feb. 2009.

[2] M. Chiani, A. Giorgetti, and E. Paolini, "Sensor radar for object tracking," *Proc. IEEE*, vol. 106, no. 6, pp. 1022–1041, Jun. 2018.

[3] Y. Wang, Q. Liu, and A. E. Fathy, "CW and pulse–Doppler radar processing based on FPGA for human sensing applications," *IEEE Trans. Geosci. Remote Sens.*, vol. 51, no. 5, pp. 3097–3107, May 2013.

[4] A. G. Yarovoy, L. P. Ligthart, J. Matuzas, and B. Levitas, "UWB radar for human being detection," *IEEE Aerosp. Electron. Syst. Mag.*, vol. 23, no. 5, pp. 36–40, Nov. 2006.

[5] V.-H. Nguyen and J.-Y. Pyun, "Location detection and tracking of moving targets by a 2D IR-UWB radar system," *Sensors*, vol. 15, no. 3, pp. 6740–6762, Mar. 2015.

[6] B. Gulmezoglu, M. B. Guldogan, and S. Gezici, "Multiperson tracking with a network of ultrawideband radar sensors based on Gaussian mixture PHD filters," *IEEE Sensors J.*, vol. 15, no. 4, pp. 2227–2237, Apr. 2015.

[7] S. Chang, R. Sharan, M. Wolf, N. Mitsumoto, and J. W. Burdick, "People tracking with UWB radar using a multiple-hypothesis tracking of clusters (MHTC) method," *Int. J. Social Robot.*, vol. 2, no. 1, pp. 3–18, Mar. 2010.

[8] D. Kocur, D. Novak, and J. Rovnakova, "Moving person tracking by UWB radar system in complex environment," in *Proc. IEEE 8th Int. Symp. Intell. Signal Process.*, Sep. 2013, pp. 77–82.

[9] J. W. Choi, X. Quan, and S. H. Cho, "Bi-directional passing people counting system based on IR-UWB radar sensors," *IEEE Internet Things J.*, vol. 5, no. 2, pp. 512–522, Apr. 2018.

[10] J. W. Choi, D. H. Yim, and S. H. Cho, "People counting based on an IR-UWB radar sensor," *IEEE Sensors J.*, vol. 17, no. 17, pp. 5717–5727, Sep. 2017.

[11] Y. Wang, J. Zhou, J. Tong, and X. Wu, "UWB-radar-based synchronous motion recognition using time-varying range-Doppler images," *IET Radar, Sonar Navigat.*, vol. 13, no. 12, pp. 2131–2139, Dec. 2019.

[12] A. Ghaffar, F. Khan, and S. H. Cho, "Hand pointing gestures based digital menu board implementation using IR-UWB transceivers," *IEEE Access*, vol. 7, pp. 58148–58157, 2019.

[13] B. Iyer, N. P. Pathak, and D. Ghosh, "Dual-input dual-output RF sensor for indoor human occupancy and position monitoring," *IEEE Sensors J.*, vol. 15, no. 7, pp. 3959–3966, Jul. 2015.

[14] S. Chang, N. Mitsumoto, and J. W. Burdick, "An algorithm for UWB radar-based human detection," in *Proc. IEEE Radar Conf. (RadarCon)*, Pasadena, CA, USA, May 2009, pp. 1–6.

[15] J. W. Choi, S. S. Nam, and S. H. Cho, "Multi-human detection algorithm-based on an impulse radio ultra-wideband radar system," *IEEE Access*, vol. 4, pp. 10300–10309, 2016.

[16] D. Miorandi, S. Sicari, F. De Pellegrini, and I. Chlamtac, "Internet of Things: Vision, applications and research challenges," *Ad Hoc Netw.*, vol. 10, no. 7, pp. 1497–1516, Sep. 2012.

[17] B. Hammi, R. Khatoun, S. Zeadally, A. Fayad, and L. Khoukhi, "IoT technologies for smart cities," *IET Netw.*, vol. 7, no. 1, pp. 1–13, Jan. 2018.

[18] H. Yamaguchi, A. Hiromori, and T. Higashino, "A human tracking and sensing platform for enabling smart city applications," in *Proc. Workshop Program 19th Int. Conf. Distrib. Comput. Netw. Workshops ICDCN*, 2018, p. 13.

[19] Y. S. Koo, L. Ren, Y. Wang, and A. E. Fathy, "UWB MicroDoppler radar for human gait analysis, tracking more than one person, and vital sign detection of moving persons," in *IEEE MTT-S Int. Microw. Symp. Dig.*, Jun. 2013, pp. 1–4.

[20] T. Higuchi, S. Fujii, H. Yamaguchi, and T. Higashino, "Mobile node localization focusing on Stop-and-Go behavior of indoor pedestrians," *IEEE Trans. Mobile Comput.*, vol. 13, no. 7, pp. 1564–1578, Jul. 2014.

[21] L. Ren and A. E. Fathy, "Noncontact heartbeat detection using UWB impulse Doppler radar," in *Proc. USNC-URSI Radio Sci. Meeting (Joint AP-S Symp.)*, Jul. 2015, pp. 1–3.

[22] Y. Xu, S. Wu, C. Chen, J. Chen, and G. Fang, "A novel method for automatic detection of trapped victims by ultrawideband radar," *IEEE Trans. Geosci. Remote Sens.*, vol. 50, no. 8, pp. 3132–3142, Aug. 2012.

[23] J. Li, L. Liu, Z. Zeng, and F. Liu, "Advanced signal processing for vital sign extraction with applications in UWB radar detection of trapped victims in complex environments," *IEEE J. Sel. Topics Appl. Earth Observ. Remote Sens.*, vol. 7, no. 3, pp. 783–791, Mar. 2014.

[24] H. Lv, W. Li, Z. Li, Y. Zhang, T. Jiao, H. Xue, M. Liu, X. Jing, and J. Wang, "Characterization and identification of IR-UWB respiratory-motion response of trapped victims," *IEEE Trans. Geosci. Remote Sens.*, vol. 52, no. 11, pp. 7195–7204, Nov. 2014.

[25] Z. Zhang, X. Zhang, H. Lv, G. Lu, X. Jing, and J. Wang, "Human-target detection and surrounding structure estimation under a simulated rubble via UWB radar," *IEEE Geosci. Remote Sens. Lett.*, vol. 10, no. 2, pp. 328–331, Mar. 2013.

[26] A. Nezirovic, A. G. Yarovoy, and L. P. Ligthart, "Signal processing for improved detection of trapped victims using UWB radar," *IEEE Trans. Geosci. Remote Sens.*, vol. 48, no. 4, pp. 2005–2014, Apr. 2010.

[27] J. Li, Z. Zeng, J. Sun, and F. Liu, "Through-wall detection of human being's movement by UWB radar," *IEEE Geosci. Remote Sens. Lett.*, vol. 9, no. 6, pp. 1079–1083, Nov. 2012.

[28] O. Boric-Lubecke, X. Gao, E. Yavari, M. Baboli, A. Singh, and V. M. Lubecke, "E-healthcare: Remote monitoring, privacy, and security," in *IEEE MTT-S Int. Microw. Symp. Dig.*, Jun. 2014, pp. 1–3.

[29] S. H. Jeong, J. E. Lee, S. U. Choi, J. N. Oh, and K. H. Lee, "Technology analysis and low-cost design of automotive radar for adaptive cruise control system," *Int. J. Automot. Technol.*, vol. 13, no. 7, pp. 1133–1140, Dec. 2012.

[30] E. Hyun and J.-H. Lee, "Multi-target tracking scheme using a track management table for automotive radar systems," in *Proc. 17th Int. Radar Symp. (IRS)*, May 2016, pp. 1–5.

[31] F. Bu and C.-Y. Chan, "Pedestrian detection in transit bus application: Sensing technologies and safety solutions," in *Proc. IEEE Intell. Vehicles Symp.*, Jun. 2005, pp. 100–105.

[32] S. Milch and M. Behrens, *Pedestrian Detection with Radar and Computer Vision*. [Online]. Available: http://www.smart-microwave-sensors.de/Pedestrian_Detection.pdf

[33] K.-T. Kim, D.-K. Seo, and H.-T. Kim, "Efficient classification of ISAR images," *IEEE Trans. Antennas Propag.*, vol. 53, no. 5, pp. 1611–1621, May 2005.

[34] M. Cristani, M. Farenzena, D. Bloisi, and V. Murino, "Background subtraction for automated multisensor surveillance: A comprehensive review," *EURASIP J. Adv. Signal Process.*, vol. 2010, no. 1, Aug. 2010, Art. no. 343057.

[35] S. Yoo, S. Chung, D.-M. Seol, and S. H. Cho, "Adaptive clutter suppression algorithm for detection and positioning using IR-UWB radar," in *Proc. 9th Int. Conf. Ultrawideband Ultrashort Impulse Signals (UWBUSIS)*, Sep. 2018, pp. 40–43.

[36] S. Singh, Q. Liang, D. Chen, and L. Sheng, "Sense through wall human detection using UWB radar," *EURASIP J. Wireless Commun. Netw.*, vol. 2011, no. 1, pp. 1–11, Jun. 2011.
[37] G. Liu, Z. Lin, S. Yan, J. Sun, Y. Yu, and Y. Ma, "Robust recovery of subspace structures by low-rank representation," *IEEE Trans. Pattern Anal. Mach. Intell.*, vol. 35, no. 1, pp. 171–184, Jan. 2013.
[38] Y. Zhang and T. Xia, "In-wall clutter suppression based on low-rank and sparse representation for through-the-wall radar," *IEEE Geosci. Remote Sens. Lett.*, vol. 13, no. 5, pp. 671–675, May 2016.
[39] J. Yin, C. Unal, M. Schleiss, and H. Russchenberg, "Radar target and moving clutter separation based on the low-rank matrix optimization," *IEEE Trans. Geosci. Remote Sens.*, vol. 56, no. 8, pp. 4765–4780, Aug. 2018.
[40] M. A. Richards, *Fundamentals of Radar Signal Processing*, 2nd ed. New York, NY, USA: McGraw-Hill, 2005, pp. 347–382.
[41] K. E. Barrett, S. M. Barman, S. Boitano, and H. Brooks, "Respiratory physiology," in *Ganong's Review of Medical Physiology*, 2nd ed. New York, NY, USA: McGraw-Hill, 2012, p. 619.
[42] H. Zeng and Y. Zhao, "Sensing movement: Microsensors for body motion measurement," *Sensors*, vol. 11, no. 1, pp. 638–660, Jan. 2011.

JI-EUN KIM received the B.S. degree in electronic engineering from Kyungpook National University, Daegu, South Korea, in 2012. She is currently pursuing the Ph.D. degree with the Radar and ElectroMagnetics Signal Processing Laboratory, Pohang University of Science and Technology (POSTECH), Pohang, South Korea. Her current research interests include measuring the clutter and target signal, analysis of the clutter signal, and target detection problems.

JAE-HO CHOI received the B.S. degree in computer science and communication engineering from Korea University, Seoul, South Korea, in 2017, and the M.S. degree in electrical engineering from the Pohang University of Science and Technology (POSTECH), Pohang, South Korea, in 2019, where he is currently pursuing the Ph.D. degree with the Radar and ElectroMagnetics Signal Processing Laboratory. His research interests include radar signal processing and pattern recognition.

KYUNG-TAE KIM received the B.S., M.S., and Ph.D. degrees in electrical engineering from Pohang University of Science and Technology (POSTECH), Pohang, South Korea, 1994, 1996, and 1999, respectively. From 2002 to 2010, he was a Faculty Member with the Department of Electronic Engineering, Yeungnam University. Since 2011, he has been with the Department of Electrical Engineering, POSTECH, Pohang, where he is currently a Professor. From 2012 to 2017, he served as the Director of the Sensor Target Recognition Laboratory, sponsored by the Defense Acquisition Program Administration and the Agency for Defense Development. He is currently the Director of the Unmanned Surveillance and Reconnaissance Technology (USRT) Research Center and the Radar and ElectroMagnetics Signal Processing (REMS) Laboratory, POSTECH. He is an author of about 300 papers on journals and conference proceedings. His research interests are mainly in the field of intelligent radar system and signal processing: SAR/ISAR imaging, target recognition, direction of arrival estimation, micro-Doppler analysis, automotive radars, digital beamforming, electronic warfare, and electromagnetic scattering. He is a member of KIEES. He was a recipient of several outstanding research awards and best paper awards from the Korea Institute of Electromagnetic Engineering and Science (KIEES) and international conferences. He is currently carrying out several research projects funded by Korean government and several industries.